AMERICAN SOCIETY FOR MICROBIOLOGY | Journal of Virology®

GENOME REPLICATION AND REGULATION OF VIRAL GENE EXPRESSION

Regulation of VP30-Dependent Transcription by RNA Sequence and Structure in the Genomic Ebola Virus Promoter

Simone Bach,[a] Jana-Christin Demper,[a] Arnold Grünweller,[a] Stephan Becker,[b] Nadine Biedenkopf,[b] Roland K. Hartmann[a]

[a]Institut für Pharmazeutische Chemie, Philipps-Universität Marburg, Marburg, Germany
[b]Institut für Virologie, Philipps-Universität Marburg, Marburg, Germany

ABSTRACT Viral transcription and replication of Ebola virus (EBOV) are balanced by transcription factor VP30, an RNA-binding protein. An RNA hairpin at the transcription start site (TSS) of the first gene (NP hairpin) in the 3′-leader promoter is thought to mediate the VP30 dependency of transcription. Here, we investigated the constraints of VP30 dependency using a series of monocistronic minigenomes with sequence, structure, and length deviations from the native NP hairpin. Hairpin stabilizations decreased while destabilizations increased transcription in the absence of VP30, but in all cases, transcription activity was higher in the presence than the absence of VP30. This also pertains to a mutant that is unable to form any RNA secondary structure at the TSS, demonstrating that the activity of VP30 is not determined simply by the capacity to form a hairpin structure at the TSS. Introduction of continuous 3′-UN_5 hexamer phasing between promoter elements PE1 and PE2 by a single point mutation in the NP hairpin boosted VP30-independent transcription. Moreover, this point mutation, but also hairpin stabilizations, impaired the relative increase of replication in the absence of VP30. Our results suggest that the native NP hairpin is optimized for tight regulation by VP30 while avoiding an extent of hairpin stability that impairs viral transcription, as well as for enabling the switch from transcription to replication when VP30 is not part of the polymerase complex.

IMPORTANCE A detailed understanding of how the Ebola virus (EBOV) protein VP30 regulates activity of the viral polymerase complex is lacking. Here, we studied how RNA sequence, length, and structure at the transcription start site (TSS) in the 3′-leader promoter influence the impact of VP30 on viral polymerase activity. We found that hairpin stabilizations tighten the VP30 dependency of transcription but reduce transcription efficiency and attenuate the switch to replication in the absence of VP30. Upon hairpin destabilization, VP30-independent transcription—already weakly detectable at the native promoter—increases but never reaches the same extent as in the presence of VP30. We conclude that the native hairpin structure involving the TSS (i) establishes an optimal balance between efficient transcription and tight regulation by VP30, (ii) is linked to hexamer phasing in the promoter, and (iii) favors the switch to replication when VP30 is absent.

KEYWORDS 3′-leader promoter, transcription start site and spacer region, RNA sequence and structure variation, switch from transcription to replication, minigenome system, qRT-PCR of viral RNAs, VP30 dependency of Ebola virus transcription

Ebola virus (EBOV) is a highly pathogenic member of the family of *Filoviridae* in the order *Mononegavirales* (1, 2). Its nonsegmented negative-sense (NNS) RNA genome, encapsidated by the nucleoprotein NP, serves as the template for viral replication and transcription of nine individual mRNAs/polypeptides encoded by seven viral genes (including three GP variants [3]). RNA synthesis is carried out by the viral RNA-dependent RNA polymerase L and its cofactor VP35 (this complex is abbreviated as RdRp

Citation Bach S, Demper J-C, Grünweller A, Becker S, Biedenkopf N, Hartmann RK. 2021. Regulation of VP30-dependent transcription by RNA sequence and structure in the genomic Ebola virus promoter. J Virol 95:e02215-20. https://doi.org/10.1128/JVI.02215-20.

Editor Rebecca Ellis Dutch, University of Kentucky College of Medicine

Copyright © 2021 American Society for Microbiology. All Rights Reserved.

Address correspondence to Roland K. Hartmann, roland.hartmann@staff.uni-marburg.de.

Received 18 November 2020
Accepted 22 November 2020
Accepted manuscript posted online 2 December 2020
Published 10 February 2021

here). Replication of negative-sense RNA genomes requires the synthesis of an intermediate antigenomic positive-sense RNA copy that serves as the template for the synthesis of new RNA genomes (4). Antigenomic RNA synthesis is initiated opposite genome position −2 (5). EBOV transcription is sequential and follows a start-stop mechanism regulated by conserved gene start (GS) and gene end (GE) sequences. It is thought that some RdRp complexes dissociate from the template RNA upon termination and can reenter the genome only at its 3′ end, which is consistent with decreasing mRNA levels, particularly for the distal VP30, VP24, and L genes (4, 6, 7).

Beyond the RdRp components L and VP35, viral transcription further requires the transcription activator VP30 (8–10). The transcription support function of VP30 is dependent on its ability to bind RNA and its phosphorylation status (11–13). Nonphosphorylated VP30 boosts transcription and simultaneously suppresses replication. Phosphorylation of VP30 increases the binding affinity for NP and decreases its affinity for RNA (12, 14). These changes in binding affinities are thought to trigger the release of VP30 from the transcription complex, resulting in a shutdown of transcription and enhancement of viral replication mediated by L and VP35 alone. Dynamic phosphorylation of VP30 at a single serine residue (Ser29) was shown to be sufficient to render VP30 active in primary transcription and to support propagation of full-length virus (11). Based on an *in vitro* study, the RNA-binding protein VP30 preferentially binds single-strand RNA (ssRNA) of mixed base composition, and inclusion of a stem-loop structure supports RNA binding by VP30 (13). Formation of a hairpin (HP) structure at the 5′ end of the first NP mRNA (Fig. 1A) was proposed to be a key feature of the VP30 dependency of transcription (15). This was inferred from Northern blot analysis of viral transcripts derived from an EBOV-specific minigenome (MG) containing an altered NP HP structure (termed NheI HP) that carried several point mutations to generate an NheI restriction site on the cDNA level. This NheI HP, with reduced stability, particularly on the mRNA level (Fig. 1A), gave rise to detectable viral mRNA synthesis even in the absence of VP30, while the original MG with the native HP strictly required VP30 for mRNA signal detection (15). This observation has been the basis for defining the functional interplay of RNA structure and VP30 during transcription initiation. The native NP HP formed by the transcription start site (TSS) and a spacer sequence, plus two additional spacer nucleotides, separates the two elements of the EBOV bipartite replication promoter (PE1 and PE2) (Fig. 1B). It has been shown that hexamer phasing between PE1 and PE2 is key to productive replication and transcription (16, 17). While it is commonly assumed that the NP HP forms posttranscriptionally in the viral mRNAs, it has been unclear whether HP formation occurs, at least transiently, at the genomic, antigenomic, and/or mRNA level during RNA synthesis by the viral RdRp. Beyond the aforementioned findings of Weik et al. (15), further indirect evidence for cotranscriptional RNA secondary structure formation was provided recently. One study revealed a novel NTPase and helicase function of VP35 (18), suggesting the need to resolve RNA structures during RNA synthesis. We showed that incremental stabilizations (particularly at the mRNA level) of HP structures in the TSS-spacer region rapidly abolish viral polymerase activity (19). This observed sensitivity of the viral RdRp led us to conclude that RNA structures are indeed able to form cotranscriptionally and that the viral RdRp is easily inhibited when such RNA structures exceed certain stability thresholds. Conversely, elimination of any RNA structure formation potential at the TSS by deletion of 12 nucleotides (nt) (Δ5′ spacer mutant) did not abrogate viral mRNA synthesis (19).

In the present study, we set out to define in more detail how RNA sequence, length, and structure in the TSS-spacer region of the genomic EBOV promoter contribute to VP30-dependent regulation of viral transcription. For this purpose, a series of monocistronic replication-competent (RC) and replication-deficient (RD) MGs (Fig. 1B) with sequence, structure, and length variations in the spacer between PE1 and PE2 were tested for reporter activity. In addition, by using quantitative reverse transcriptase PCR (qRT-PCR), the levels of different viral RNA were quantified: mRNA, genomic RNA (viral

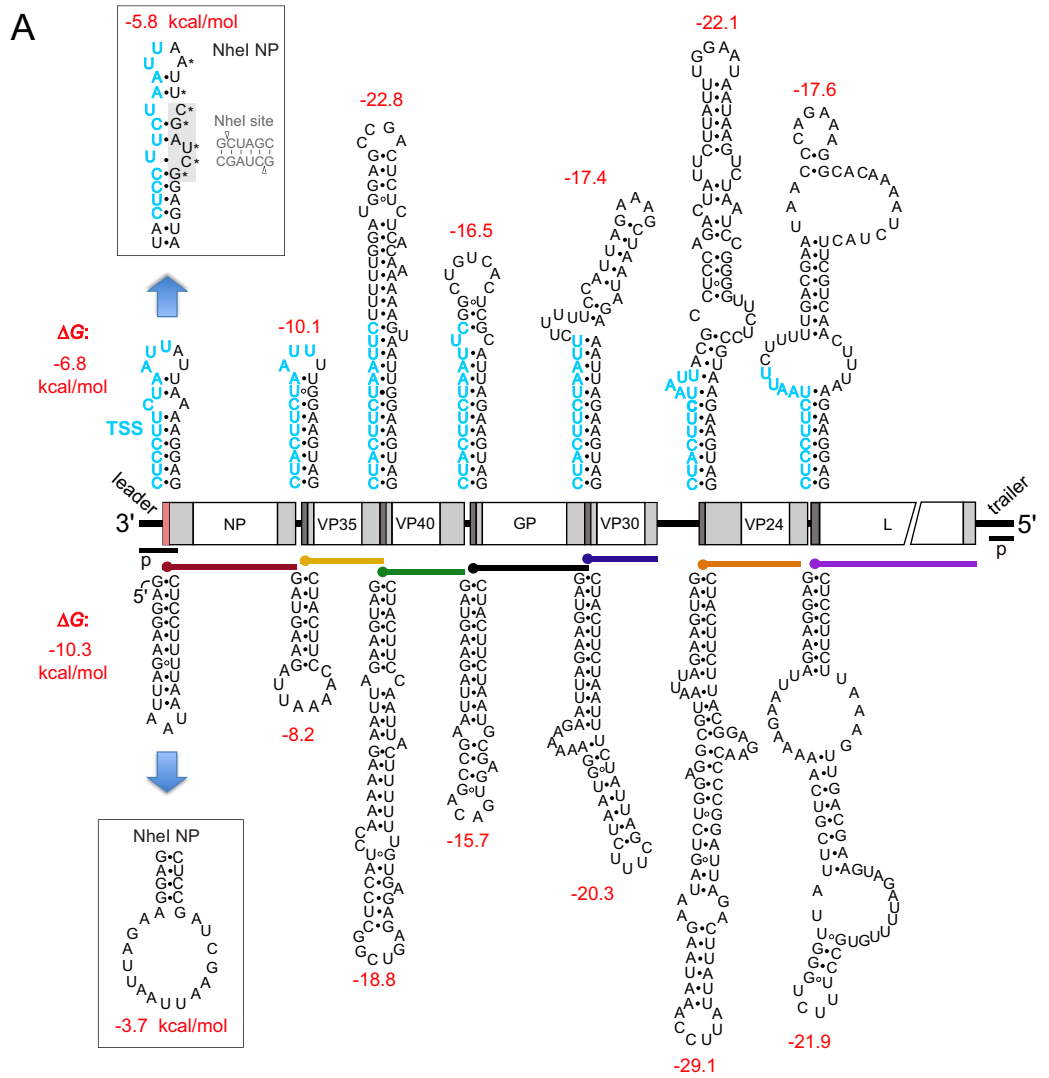

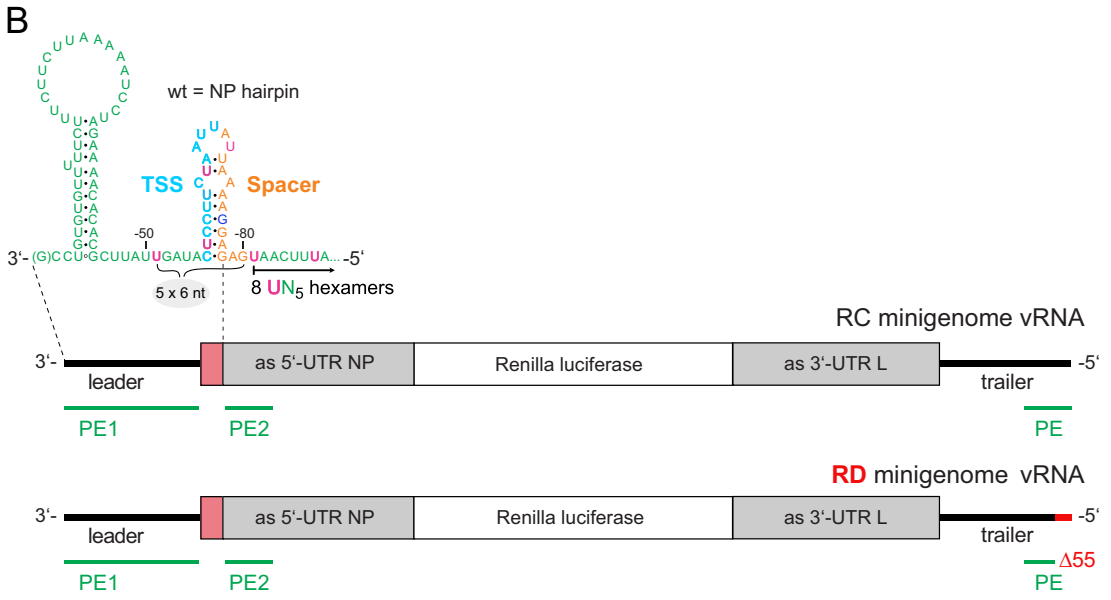

FIG 1 (A) Architecture of the negative-sense EBOV genome (vRNA). Potential secondary structures at the 3′-end and internal transcription start regions are depicted at the top. The transcription start sequence (TSS) of the first NP gene and gene start

(Continued on next page)

RNA [vRNA]), and antigenomic RNA (cRNA). In all cases, reporter activity and viral RNA levels were directly compared for cells cotransfected with and without the plasmid encoding VP30.

RESULTS

Spacer mutants show partial enhancements of viral transcription in the absence of VP30. Substantial VP30-independent transcription observed for an MG with the NheI NP mutation has been the basis for the model that hairpin stability at the TSS defines the control of transcription by VP30 in the EBOV system (15). We set out to scrutinize this assumption by analyzing viral RNA synthesis for a series of MGs that varied in HP length and predicted stability in the presence versus absence of VP30. These variant MGs were constructed by replacing the native NP HP at the transcription initiation region in the 3′-leader with corresponding HP structures derived from internal EBOV genes (Fig. 2; see Fig. S1 in the supplemental material for predicted HP stabilities at the genomic and antigenomic RNA level). In all replacement constructs except for the VP40 HP variant, nucleotides were inserted or deleted to maintain hexamer phasing ($n \times 6$ nt) between nt −51 of PE1 and nt −80 of PE2 (Fig. 1B) without significantly changing the authentic HP structures (e.g., cf. the native VP35 HP in Fig. 1A with the VP35+1 derivatives in Fig. 2 and Fig. S1). The engineered HPs of the internal EBOV genes preserved a functional TSS, represent sequence/structural elements that are efficiently utilized by the EBOV RdRp, and were previously demonstrated to basically support initiation of viral RNA synthesis (17). In addition, we included the NheI and Δ5′ spacer mutants (Fig. 2); the latter mutant, which lacks 12 spacer nucleotides, is unable to form any secondary structure at the negative-sense or positive-sense RNA level.

The replication-competent minigenomes (RC MGs), cotransfected with or without VP30, were analyzed in luciferase reporter assays (Fig. 3A). Activities in the presence of VP30 varied among the spacer variants (Fig. 3A, white bars; wt NP MG in gray), in line with data reported recently (17). Interestingly, in the absence of VP30, all tested RC MG mutants gave rise to reporter activities exceeding that of the MG encoding the native NP HP (Fig. 3A, blue bars). This indicates that the native NP HP is optimized for tight regulation by VP30. Furthermore, the extent of viral transcription in the absence of VP30 differed considerably between MG mutants, and there is no simple correlation between HP structure formation at the TSS and VP30 dependency, as previously suggested for the NheI HP mutant (15). This is illustrated by the Δ5′ spacer mutant, which is unable to form any RNA secondary structure at the TSS. This variant showed even lower levels of reporter activity in the absence of

FIG 1 Legend (Continued)
(GS) sequences of the six internal EBOV genes are in light blue. Corresponding hairpin structures are also predicted to form on the mRNA level (illustrated at the bottom). The previously reported NheI mutant of the NP HP (15) is illustrated above and below the native NP HP; in the genomic sequence of the NheI NP variant at the top, the mutations are indicated by asterisks and the NheI site generated on the cDNA levels is depicted next to the corresponding RNA sequence stretch (gray shaded). Schematic white boxes in the center mark the reading frames for EBOV proteins NP, VP35, VP40, GP, VP30, VP24, and L; 5′- and 3′-untranslated regions (UTRs) are depicted as light gray boxes, with dark gray areas marking the positions of the predicted secondary structures illustrated above and below the genome. The box representing the first NP hairpin structure is in red; mRNAs are illustrated as colored lines, with dots indicating the 5′-cap. p, genomic 3′-leader and antigenomic trailer promoters (26). The secondary structures are the minimum free energy (MFE) structures (predicted by RNAfold [27] using the default parameters; http://rna.tbi.univie.ac.at/cgi-bin/RNAWebSuite/RNAfold.cgi); their stabilities (ΔG values, in kilocalories per mole), depicted in red, were calculated with one single-stranded residue included on the 5′-side (genomic RNA) and on the 3′-side (genomic RNA and mRNA) of the stem base. (B) Illustration of the replication-competent (RC; top scheme) and replication-deficient (RD; bottom scheme) minigenome (MG) skeleton used in this study; the secondary structure potential at the genomic 3′ end is depicted above the top scheme, which was validated by structure probing of naked RNA *in vitro* (13, 15, 16). RD MGs lack the trailer promoter's terminal 55 nt (depicted in red), thus restricting RNA synthesis to primary transcription and antigenome synthesis. PE, promoter elements (in green); the genomic replication promoter is bipartite, consisting of PE1 and PE2. Bold pink letters highlight the 3′-U residues of 3′-UN_5 hexamers between PE1 and PE2 (17). The TSS and PE2 are separated by a spacer region (orange letters). Negative values are used for nucleotide numbering of the genomic negative-sense RNA, reflecting the genome's 3′-to-5′ negative-sense orientation. The genomic 3′-terminal G is depicted in parentheses as its presence is not essential for initiation of antigenomic RNA synthesis by the EBOV RNA polymerase complex (5). Gray boxes in the schematic genome representation represent sequences antisense (as) to the 5′-UTR of the NP mRNA and antisense to the 3′-UTR of the L mRNA.

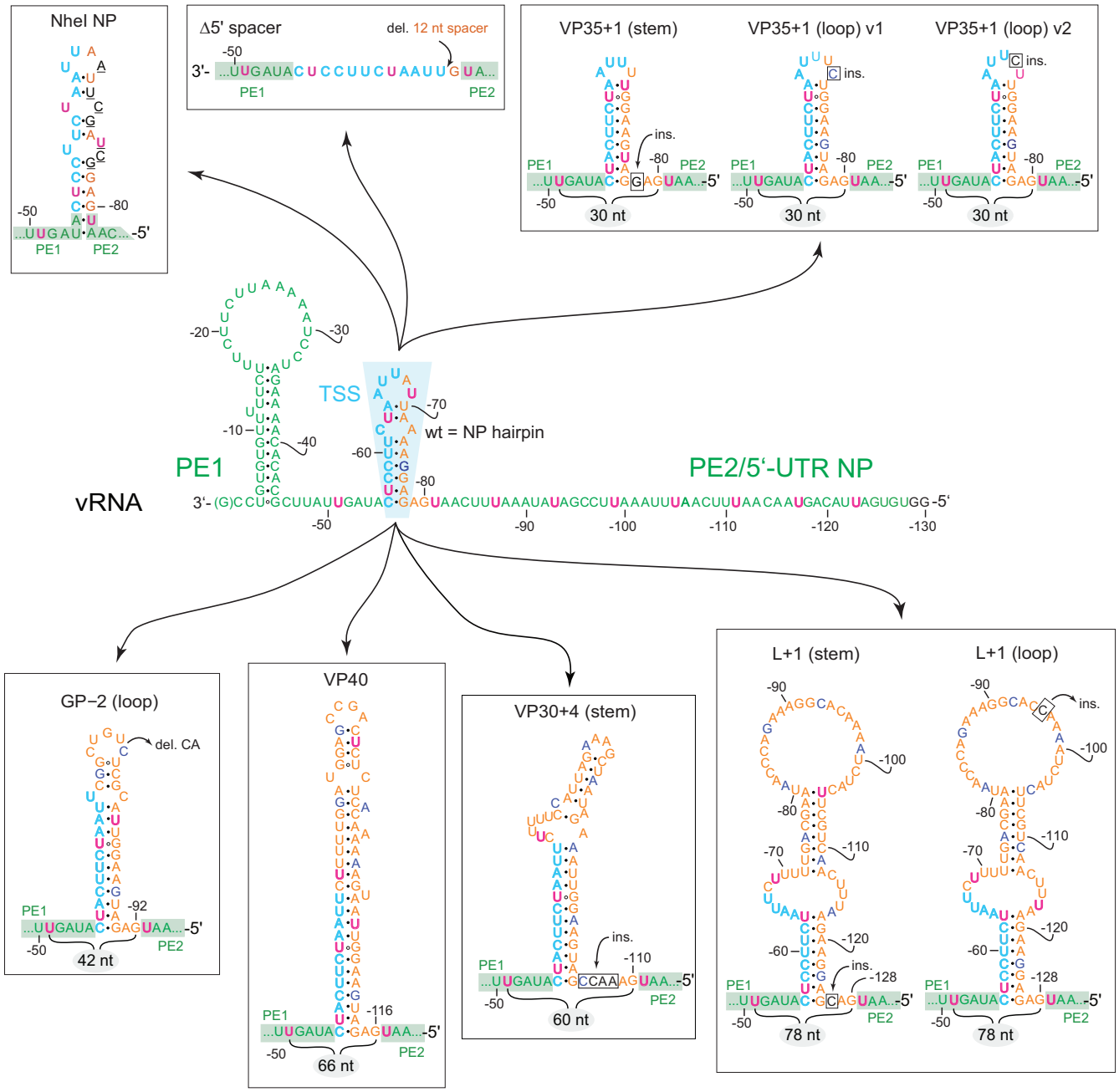

FIG 2 Illustration of MG variants analyzed in Fig. 3. The genomic (vRNA) 3′-leader encoding the native wt NP hairpin (HP) structure (area shaded in light blue) is shown in the center. The NP HP was either changed by mutation (variant NheI NP) or deletion (variant Δ5′ spacer) or replaced with (engineered) HP structures derived from GS regions of internal EBOV genes. For color coding, see the legend to Fig. 1B. Hexamer periodicity between PE1 and PE2 is depicted for each variant by highlighting of the pink 3′-U residues of 3′-UN_5 hexamers and the nucleotide distance between positions −51 and −80, which is a multiple of six in all variants shown. Nucleotides of PE1 and PE2 are shaded in green. MG variants with HP structures derived from GS regions of internal EBOV genes (except for the VP40 HP) were adjusted to hexamer phasing by inserting (boxed nucleotides) or deleting nucleotides, either at the 5′-side of the hairpin stem or in its apical loop. ins., insertion; del., deletion. Underlined nucleotides in the NheI hairpin mark point mutations relative to the wt NP HP.

VP30 than constructs with clear HP formation potential, such as the VP35+1 (loop) variants and the VP40 construct (Fig. 3A). Also the L+1 (stem) and L+1 (loop) variants with very similar structure formation potential at the negative-sense or positive-sense RNA level differed considerably in reporter activity when VP30 was absent (see below). The two VP35 hairpin constructs [VP35+1 (loop) v1 and v2], with single C residues inserted into the apical loop at either genome position −69 or −68 to maintain hexamer phasing (Fig. 2), displayed the highest levels of

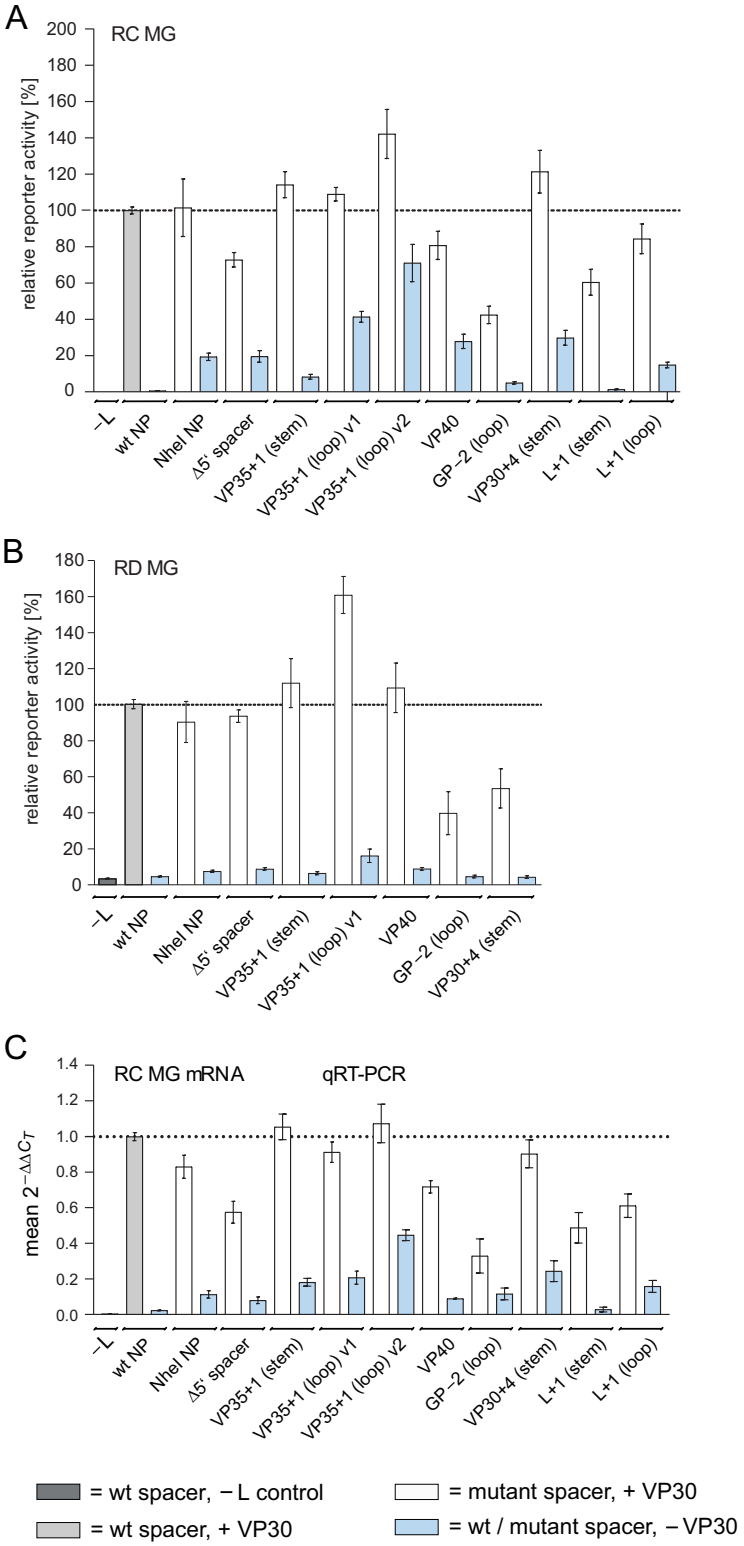

FIG 3 (A) Reporter gene activity of RC MG variants specified in Fig. 2 and transfected together with a plasmid expressing VP30 (gray and white bars) or omitting such a plasmid (light blue bars). The upper dotted line represents the respective activity value for the MG carrying the native 3′-leader (wt NP), which was set to 100% (gray column). −L, background control, i.e., MG transfection without the plasmid encoding the polymerase L. (B) Reporter gene activity of corresponding constructs as part of the RD MG. Values (± SEM) in panel A and B are based on at least 3 biological replicates with 2 or 3 technical replicates each. (C) qRT-PCR analysis of mRNA levels in selected samples obtained from the

(Continued on next page)

reporter activity in the absence of VP30 (41% and 71%, respectively, relative to the wild-type [wt] NP MG in the presence of VP30; Fig. 3A).

As reporter assays of RC MGs cannot disentangle effects on viral transcription and replication, we also tested several of the mutant constructs as part of a replication-deficient minigenome (RD MG) (Fig. 1B and 3B). In the RD MG context, viral mRNA synthesis takes place only on nucleocapsids containing the vRNA synthesized by the T7 RNA polymerase, without the enhancing effect of viral replication. We basically observed the same trends for the RD MGs (Fig. 3B) as seen for the RC MGs (Fig. 3A), although the extent of reporter activity in the absence of VP30 was generally lower in the RD MG background. For example, variant VP35+1 (loop) v1 gave 12.8% (after subtraction of the −L background) (Fig. 3B) reporter activity when VP30 was absent compared with ~41% in the RC MG background (Fig. 3A).

To determine viral mRNA levels directly rather than relying on indirect reporter activity readouts, we performed qRT-PCR experiments (Fig. 3C) using total RNA derived from the same cells that were used for the analysis of reporter activity in Fig. 3A. qRT-PCR quantification of mRNAs basically confirmed the relative pattern of reporter activities, although mRNA levels tended to be more reduced in the absence of VP30 than RC MG reporter activities (cf. Fig. 3A and C). For example, mRNA levels were 21% (Fig. 3C) for variant VP35+1 (loop) v1 compared with 41% in Fig. 3A, relative to the wt NP 3′-leader construct in the presence of VP30 (= 100%); likewise, the percentages were 45% versus 71% for variant VP35+1 (loop) v2 and or 11% versus 19% for the NheI NP variant. We conclude that RC and RD MG reporter activities provide comparative estimates of viral transcription, but only qRT-PCR allows reliable quantification of viral mRNA amounts. RC MG reporter activities tend to overestimate viral transcription, and RD MG reporter activities have the drawback of lower activities (low signal-to-noise ratio), which also prevents reliable qRT-PCR quantification of viral mRNAs in RD MG-transfected cells (19).

Overall, the results presented in Fig. 3 show that the majority of the tested spacer variants gave rise to increased reporter activity/viral mRNA transcription in the absence of VP30 compared to the native NP HP construct, but none resulted in completely VP30-independent viral transcription. We conclude that the native spacer/NP HP is optimized for tight regulation of transcription initiation by VP30. The observation of an only moderate extent of transcription in the absence of VP30 in the case of the Δ5′ spacer variant lacking any RNA structure at the TSS indicates that HP formation and stability at the TSS are not the single key determinant of VP30 dependency.

Increased RNA secondary structure stability reduces transcription with and without VP30. We next addressed the correlation between VP30 dependency of transcription and RNA hairpin stability at the TSS more specifically by focusing on spacer mutants with enhanced HP stability relative to the native leader MG. For this purpose, we chose the previously characterized (19) VP40 variant and two incrementally yet moderately stabilized versions of this hairpin (termed $VP40_5$ and $VP40_6$), as well as the NP G_{-72} mutant, a stabilized variant of the authentic NP HP owing to a point mutation (Fig. 4A). The NP G_{-72} mutant showed a further reduction of reporter activity in the absence of VP30 relative to the wt NP MG (Fig. 4B); qRT-PCR quantification of mRNA levels then revealed that mRNA levels were decreased not only in the absence but also in the presence of VP30 relative to the respective wt NP control (Fig. 4C). Without VP30, the VP40 HP construct showed substantially increased levels of reporter activity and, to a lesser extent, increased mRNA levels (Fig. 4B and C). This phenotype tended to attenuate for the $VP40_6$ variant, which differed from the native VP40 HP by conversion of a predicted C·U mismatch into a G·C base pair in the upper stem region (Fig. 4A). The second $VP40_5$ variant, predicted to further increase stem

FIG 3 Legend (Continued)
same kind of RC MG-transfected cells as analyzed in panel A. Mean $2^{-\Delta\Delta C_T}$ values as a measure of mRNA levels relative to the wt NP MG, based on at least 3 independent experiments with a total of 2 or 3 technical replicates each. For details on the qRT-PCR setup, see Materials and Methods.

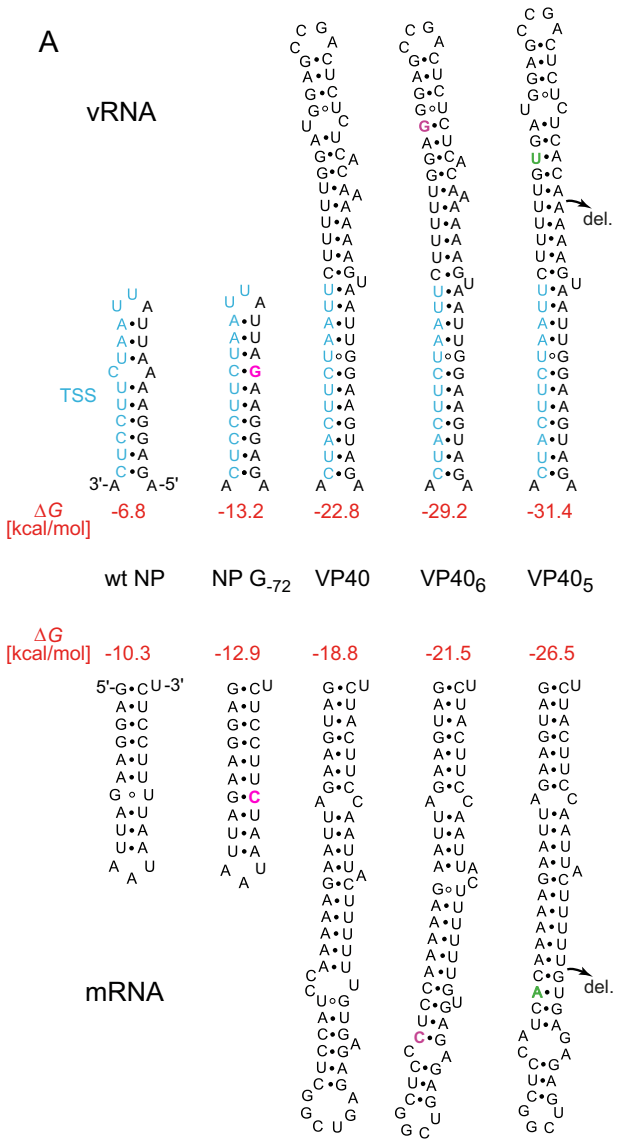

FIG 4 (A) RNA secondary structure potential of stabilized variants of the wt NP HP (variant NP G_{-72}) or the VP40 HP (variants $VP40_5$ and $VP40_6$, constructed as part of a series of VP40 HP variants [19]). Predicted MFE structures (RNAfold; for more details, see the legend to Fig. 1A) and their ΔG values (in kilocalories per mole; red) are shown at the genomic (vRNA) or mRNA level. The TSS is in light blue, point mutations (relative to the parental native structure) are in pink, nucleotide insertions are in green, and deletions (del.) are shown by arrows. (B to E) Influence of RNA secondary structure stabilization at the TSS on reporter activity and viral RNA synthesis in the presence and absence of VP30. (B) Luciferase reporter gene assays of the RC MG constructs illustrated in panel A. The mean activity value for the wt NP MG was set to 100%. Mean relative reporter gene activity values ± SEM were derived from at least 3 independent experiments with 3 technical replicates each. (C to E) Corresponding qRT-PCR analyses for the quantification of mRNA, cRNA, and vRNA levels in total RNA samples derived from the MG-transfected cells that were analyzed for reporter activity in panel B. Values are based on 3 independent experiments with 3 technical replicates each. $2^{-\Delta\Delta C_T}$ values were normalized to RNA levels measured for the wt NP MG ($2^{-\Delta\Delta C_T} = 1$). *, $P < 0.05$; **, $P < 0.01$; ***, $P < 0.001$; ****, $P < 0.0001$ (unpaired t test with Welch's correction). For more details, see Materials and Methods.

stability, particularly at the mRNA level, owing to an additional U·A base pair and deletion of a bulged A residue, already showed a marked reduction in VP30-independent reporter activity and mRNA levels (Fig. 4B and C). However, mRNA levels were also decreased to ~25% in the presence of VP30 (Fig. 4C). We conclude from the findings presented in Fig. 4 that even minor stabilizations of hairpin structures at the

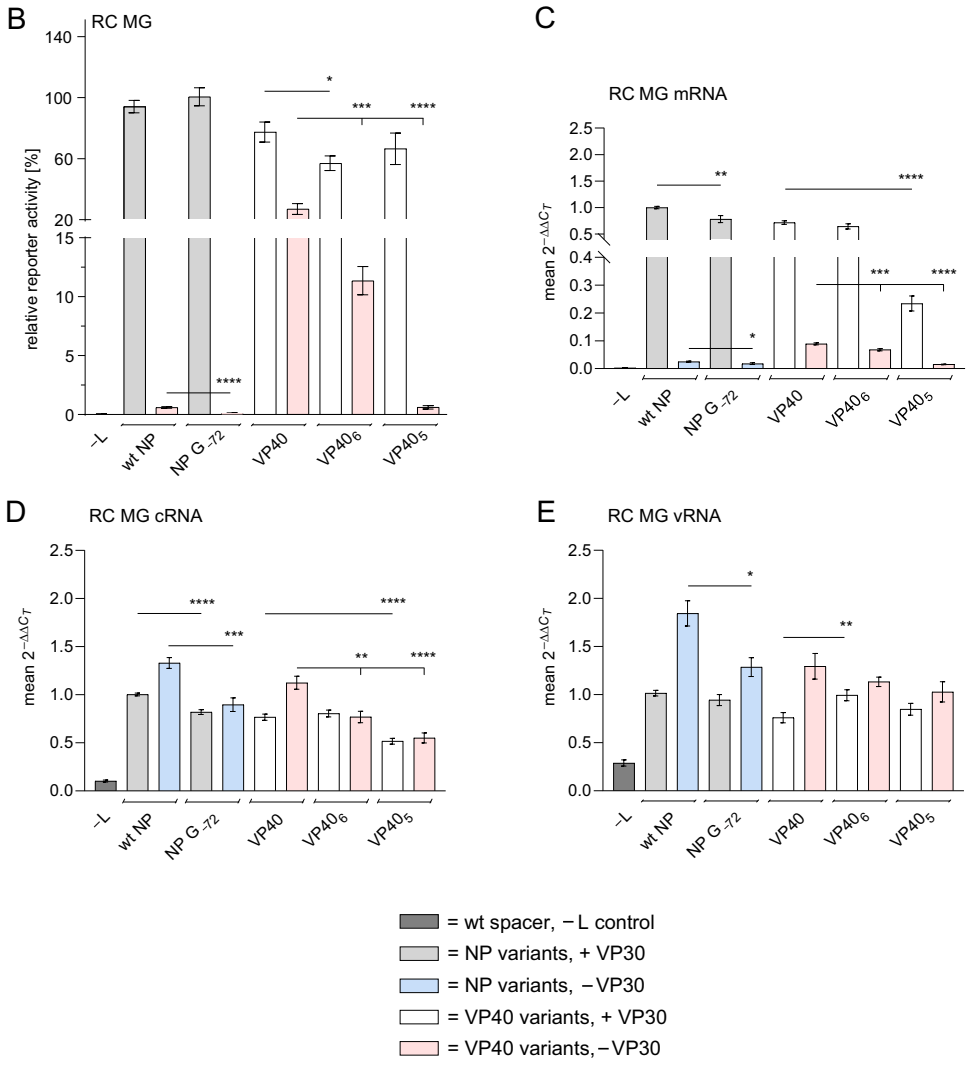

FIG 4 (Continued)

TSS rapidly reduce viral transcription efficiency in the absence of VP30, but also in its presence.

RNA secondary structure stabilization reduces cRNA synthesis in the presence and absence of VP30. Quantification of cRNA and vRNA levels for the MGs analyzed in Fig. 4 revealed that the relative increase of cRNA synthesis seen for the wt NP MG upon omission of VP30 was dampened in the case of the stabilized variant NP G_{-72} (Fig. 4D). The same pertains to the $VP40_5$ and $VP40_6$ mutants relative to the VP40 construct. This trend was also evident in the relative vRNA levels (Fig. 4E). Finally, in the presence of VP30, all mutant constructs, including the VP40 variant, yielded lower cRNA levels than the wt NP MG (gray and white bars in Fig. 4D).

The G-to-U_{-75} point mutation boosts transcription and abrogates the switch from transcription to replication in the absence of VP30. We next investigated whether 3′-UN_5 hexamer phasing between PE1 and PE2 may affect the VP30 control of transcription. A G_{-75}-to-U mutation in the NP hairpin, making the UN_5 hexamer phasing continuous between PE1 and PE2, enhanced the efficiency of transcription and replication in the presence of VP30 (17). This also pertains to variant NP U_{-75}/G_{-72} with an additional mutation (G_{-72}) to counteract the destabilizing effect of the U_{-75} mutation on hairpin formation on the genomic and antigenomic level (Fig. 5A). The two MG

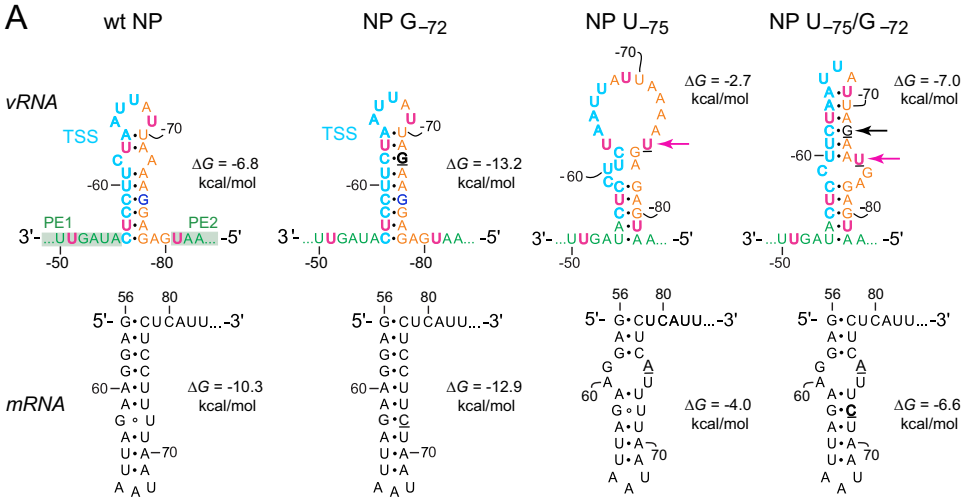

FIG 5 Effects of NP hairpin destabilization as well as continuous hexamer periodicity between PE1 and PE2 on reporter activity and viral RNA levels in the presence versus absence of VP30. (A) Predicted secondary structures on the genomic and mRNA level for the wt NP HP and variants NP G_{-72}, NP U_{-75}, and NP U_{-75}/G_{-72}. For details on color coding, see Fig. 1B and 2. ΔG values of the MFE structures predicted by RNAfold using the default parameters are indicated (for more details, see the legend to Fig. 1A). Exchanged nucleotides in the mutant structures are underlined. In the NP U_{-75} and U_{-75}/G_{-72} variants, horizontal arrows additionally highlight the point mutation at position −75 (pink) and the stabilizing point mutations at −72 (black). For genomic RNA (vRNA), numbers with minus signs and for mRNA the same numbers with plus signs were used, counting from the genome 3′ end. (B and C) Luciferase reporter gene assays of RC (B) and RD (C) MG variants illustrated in panel A and Fig. 2. Reporter activities relative to those of the wt NP MG (set to 100%) are given, based on at least 3 biological replicates (± SEM) with 2 or 3 technical replicates each. (D to F) Corresponding qRT-PCR analyses of total RNA samples derived from the cells analyzed in panel B, specific for (D) mRNA, (E) antigenomic/copy RNA (cRNA), and (F) genomic/viral RNA (vRNA). Red numbers in panel D represent mean *n*-fold activity increases relative to the wt NP MG, in the absence of VP30. Mean $2^{-\Delta\Delta C_T}$ values ± SEM are derived from at least three independent experiments with two or three technical replicates each. *, $P < 0.05$; **, $P < 0.01$; ***, $P < 0.001$; ****, $P < 0.0001$ (unpaired *t* test with Welch's correction). For more details, see Materials and Methods.

variants enhanced reporter activity in the RC and RD MG background not only in the presence of VP30 but also in the absence of VP30 relative to the wt NP, NheI NP, and Δ5′ spacer MGs (Fig. 5B and C). This is consistent with increased mRNA levels determined by qRT-PCR (Fig. 5D). Remarkably, reporter activity of the NP U_{-75}/G_{-72} MG without VP30 exceeded that of the wt NP MG with VP30 (Fig. 5B). As already observed in Fig. 3, relative reporter activities in the absence of VP30 were higher in the RC MG setup than in the RD MG system (Fig. 5C) or at the mRNA level (Fig. 5D). Nevertheless, the NP U_{-75}/G_{-72} MG with continuous hexamer phasing and moderate HP stability showed the second highest level of VP30-independent transcription among all tested constructs [~36% (Fig. 5D); variant VP35+1 (loop) v2, 45% (Fig. 3C)].

We also determined the cRNA and vRNA levels for the RC MG variants analyzed in Fig. 5B to D. The wt NP, NheI NP, and Δ5′ spacer MGs showed increased cRNA and vRNA levels in the absence of VP30, in line with a switch from transcription to replication when VP30 is absent (Fig. 5E and F). Remarkably, such an increase in the absence of VP30 was largely attenuated for the NP U_{-75} and NP U_{-75}/G_{-72} mutants. In summary, both mutants, despite their differences in HP stability, boost transcription, particularly in the absence of VP30, and additionally abrogate the switch from transcription to replication in the absence of VP30.

The level of VP30-independent transcription observed for the NP U_{-75} and U_{-75}/G_{-72} variants exceeds that of the Δ5′ spacer variant (Fig. 5D), although the latter is unable to form any structures at the TSS and also has the feature of continuous hexamer phasing between PE1 and PE2 (Fig. 2). We suspect that the phenotype of the Δ5′ spacer variant is dominated by an intrinsic defect for which its reduced mRNA, cRNA, and vRNA levels in the presence of VP30 may be taken as evidence (Fig. 5D to F). The

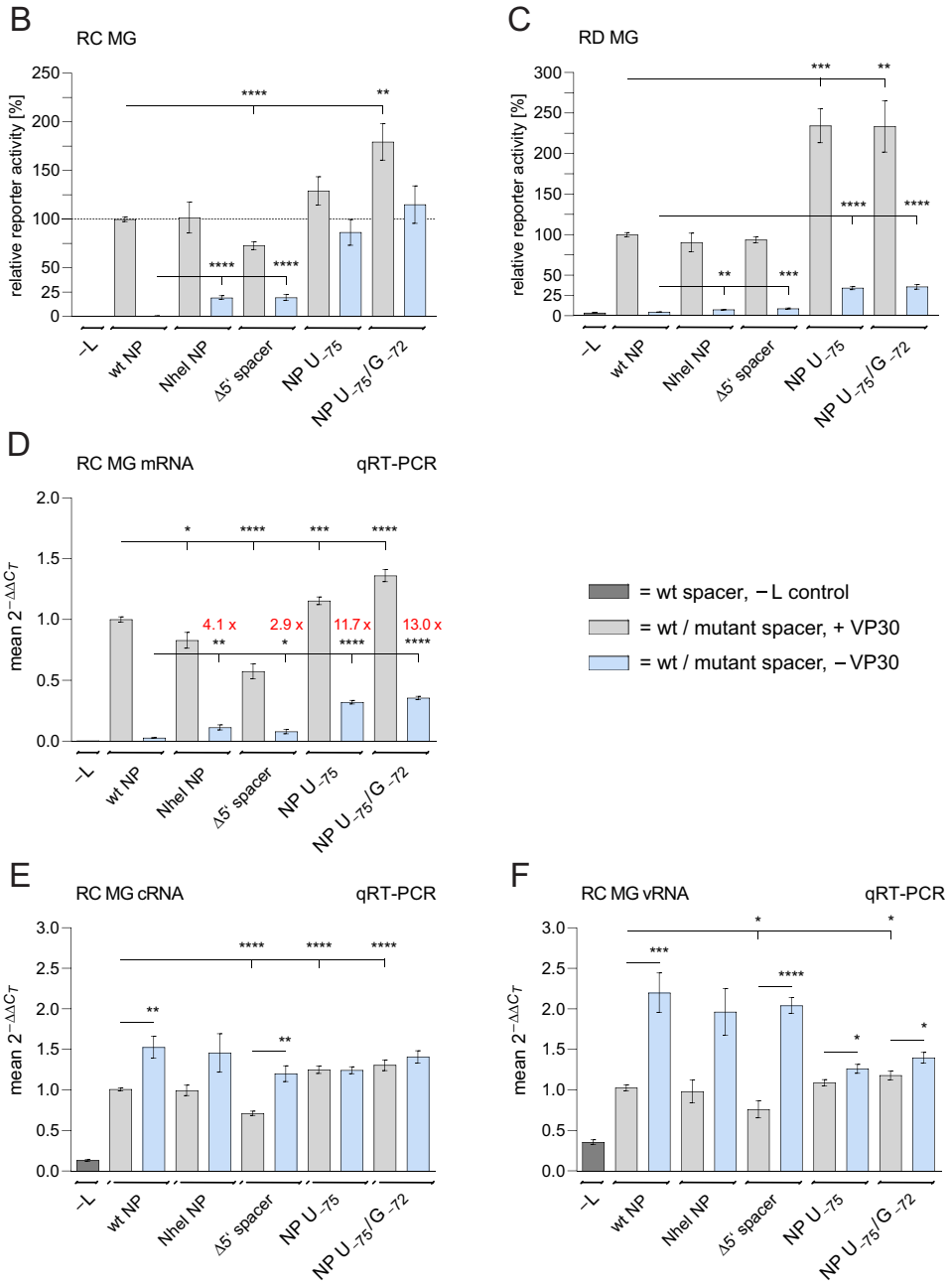

FIG 5 (Continued)

defect might be related to a less defined or suboptimal distance between PE1 and PE2 in the absence of any stem-loop structure; however, this is speculative at present and has to be addressed in future studies.

VP30 can support a low level of viral transcription when hexamer phasing is violated. To investigate the role of hexamer phasing between PE1 and PE2 for transcription and replication in the presence versus absence of VP30, we quantified the mRNA, cRNA, and vRNA levels for MG constructs that either maintained hexamer phasing between genome positions −51 and −80 [wt NP, VP35+1 (loop) v1, and GP−2 nt PE1] or not [VP35 and NP−1 (stem)] (Fig. 6A). Variant NP−1 (stem) was chosen because this construct was isosequential to the native wt NP construct, and the pair VP35+1 (loop) v1 and VP35 was chosen because their HP size was comparable to that of the wt HP and because variant VP35+1 (loop) v1 showed substantially increased transcription

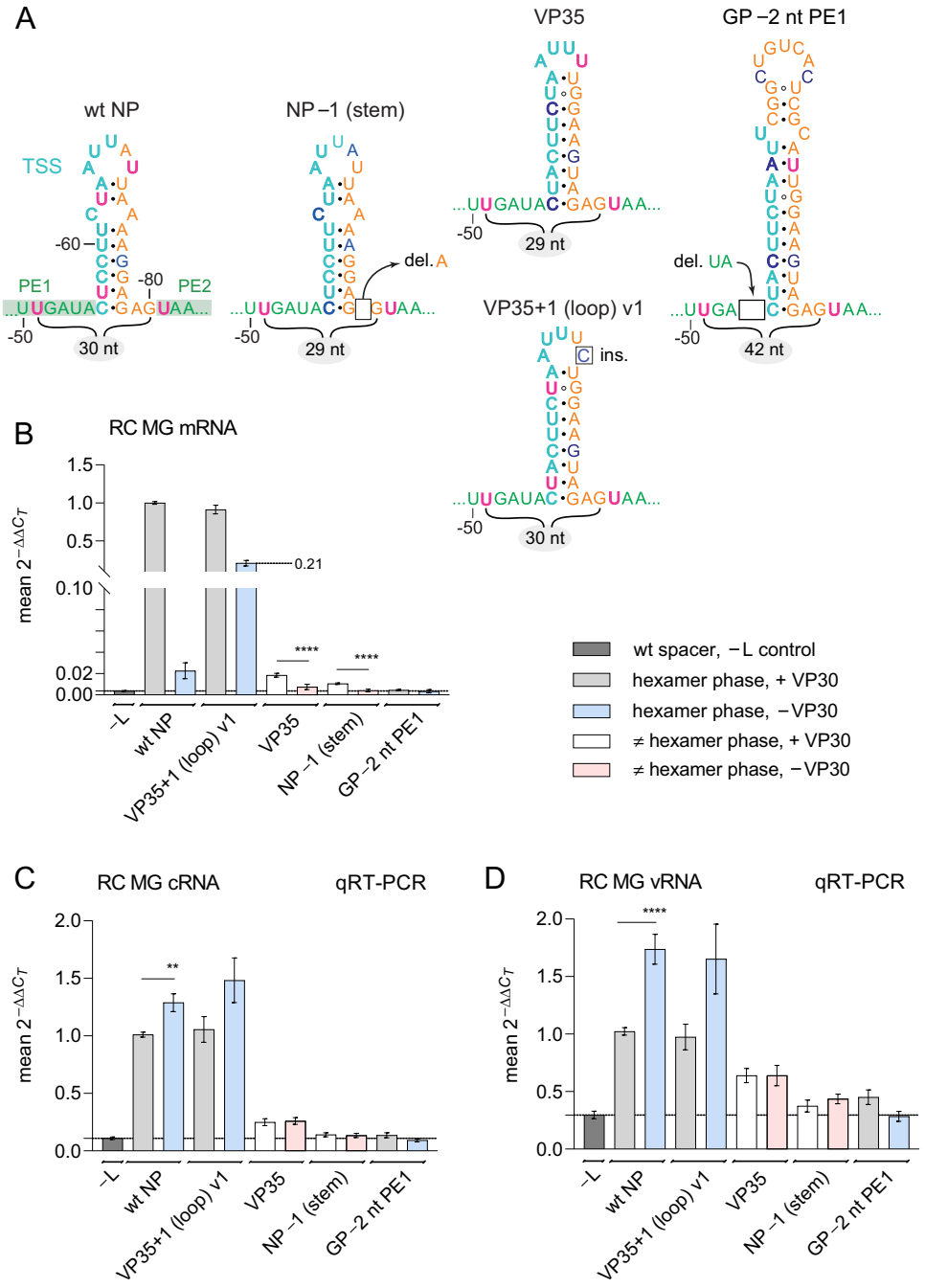

FIG 6 Effects of VP30 on MGs deviating from hexamer phasing between PE1 and PE2. (A) Predicted TSS-spacer structures of MG variants that either do [wt (NP) and VP35+1 (loop) v1] or do not [VP35, NP−1 (stem), and GP−2 (Δ2 nt PE1)] conform to hexamer phasing. In variant GP−2 (Δ2 nt PE1), genome nucleotides −54 and −55 of PE1 are deleted (17). Insertions or deletions of nucleotides are marked by boxes. ins., insertion; del., deletion. For the color code, see the legend to Fig. 1B. (B to D) Corresponding qRT-PCR analyses of total RNA obtained from cells transfected with the RC MGs illustrated in panel A, distinguishing between relative amounts of (B) viral mRNA, (C) cRNA, and (D) vRNA. Mean $2^{-\Delta\Delta C_T}$ values ± SEM are derived from at least 3 independent experiments with 2 or 3 technical replicates each. **, $P < 0.01$; ****, $P < 0.0001$ (unpaired t test with Welch's correction). The dotted lines mark the level of the −L controls. For more details, see Materials and Methods.

in the absence of VP30 (Fig. 3C and 6B). Variant GP−2 nt PE1 was included because it carried a deletion of nt −54 and −55 of PE1, directly upstream of the TSS (position −56), which altered the distance of the TSS to the genome 3′ end, although hexamer phasing between PE1 nt −51 and PE2 was maintained (Fig. 6A). In the absence of

VP30, mRNA levels of constructs VP35, NP−1 (stem), and GP−2 nt PE1 were essentially as low as the background (−L) control (Fig. 6B). However, in the presence of VP30, mRNA levels of the VP35 and NP−1 (stem) mutants were still low but clearly above the (−L) control. This finding suggests that low-efficiency transcription of viral mRNA can occur with support of VP30 despite violation of hexamer periodicity between PE1 and PE2. In contrast, there was not even a minor rescue of mRNA synthesis in the presence of VP30 in the case of the GP−2 nt PE1 variant (Fig. 6B). This is in line with the recent finding that deletion of nucleotides −54 and −55 completely abolishes transcription, either because the two nucleotides are an essential part of the EBOV transcription promoter required for binding of the transcriptase complex or because the TSS must be in the correct hexamer phase relative to the genome 3′ end (17); yet another possibility could be that the genome nucleotide at the transcription initiation site (C_{-56}) needs to bind to NP in a specific phase, as was suggested for Sendai virus (*Paramyxoviridae*) (20).

For cRNA and vRNA synthesis (Fig. 6C and D), several aspects are worth mentioning: (i) basic levels of cRNA and vRNA synthesis above background can occur despite disruption of hexamer phasing, as was evident for the VP35 HP construct; (ii) this low-efficiency replication was barely affected by the presence of VP30; (iii) the GP−2 nt PE1 construct apparently still allowed VP30-dependent synthesis of very low cRNA levels that in turn gave rise to vRNA synthesis that was modest but clearly above the (−L) background; (iv) for the VP35 HP construct, cRNA levels were ~8-fold lower (+ VP30, Fig. 6C) than for the wt NP MG (after subtraction of −L background), but vRNA levels were only ~2-fold lower (Fig. 6D, + VP30). Evidently, vRNA synthesis is less affected than mRNA or cRNA synthesis by violation of hexamer periodicity at the genomic 3′-leader promoter. A possible explanation is that viral polymerases that failed to initiate RNA synthesis at the genomic promoter become increasingly available for replication initiation at the antigenomic promoter. Finally, the extent of residual mRNA, cRNA, and vRNA synthesis in MG constructs disrupting hexamer periodicity depends on the sequence/structure context [cf. variants VP35 and NP−1 (stem) (Fig. 6B to D)].

Spacer expansions of up to 66 nt still allow detectable VP30-independent transcription. We previously showed that extension of the PE1/PE2 spacer region by up to 66 nt still allowed substantial viral RNA synthesis (~25% of wt NP) in the presence of VP30 in the RC MG system (19). Here, we assessed how MG constructs with increasing spacer expansions respond to the absence of VP30 (Fig. 7A). The analysis included 3′-leader variants in which the NP HP was replaced with the VP40 HP and derivatives thereof with insertions of up to 5 × 6 nt, with the longest variant, VP40+30, expanding the spacer region by 66 nt (Fig. 7B). Furthermore, we included the VP24−4 (19) and the two L+1 variants with insertions of 48 nt for comparison (Fig. 7B). The relatively high level of reporter activity in the absence of VP30 for the VP40 construct also remained quite constant for variants VP40+6, VP40+12, and VP40+18 and was similar to that of the VP24+4 variant, with spacer length equal to that of the VP40+12 construct (Fig. 7A). Variants VP40+24 and VP40+30 showed decreased activity without VP30 but also lowered activity in the presence of VP30, in line with reduced mRNA levels (19), suggesting that expansions of 60 and more nucleotides in the spacer between PE1 and PE2 begin to decrease the proportion of polymerases that are able to recognize the genomic promoter. However, for polymerases that succeed in initiating transcription, the support function of VP30 appears to be unchanged despite the spacer extensions.

A clear difference in reporter activity/mRNA levels (Fig. 3A and C) with and particularly without VP30 was observed for the variants L+1 (stem) versus L+1 (loop), which have the same spacer length but differ in the position of their 1-nt insertion (either in the loop or at the base of the stem) to maintain hexamer phasing. As this 1-nt insertion at the two different positions is unlikely to substantially affect the stability of the hairpin structure (Fig. 7B), we consider two explanations possible: either the difference in the positioning of one UN_5 hexamer [U_{-105} in variant L+1 (stem), U_{-117} in variant L+1

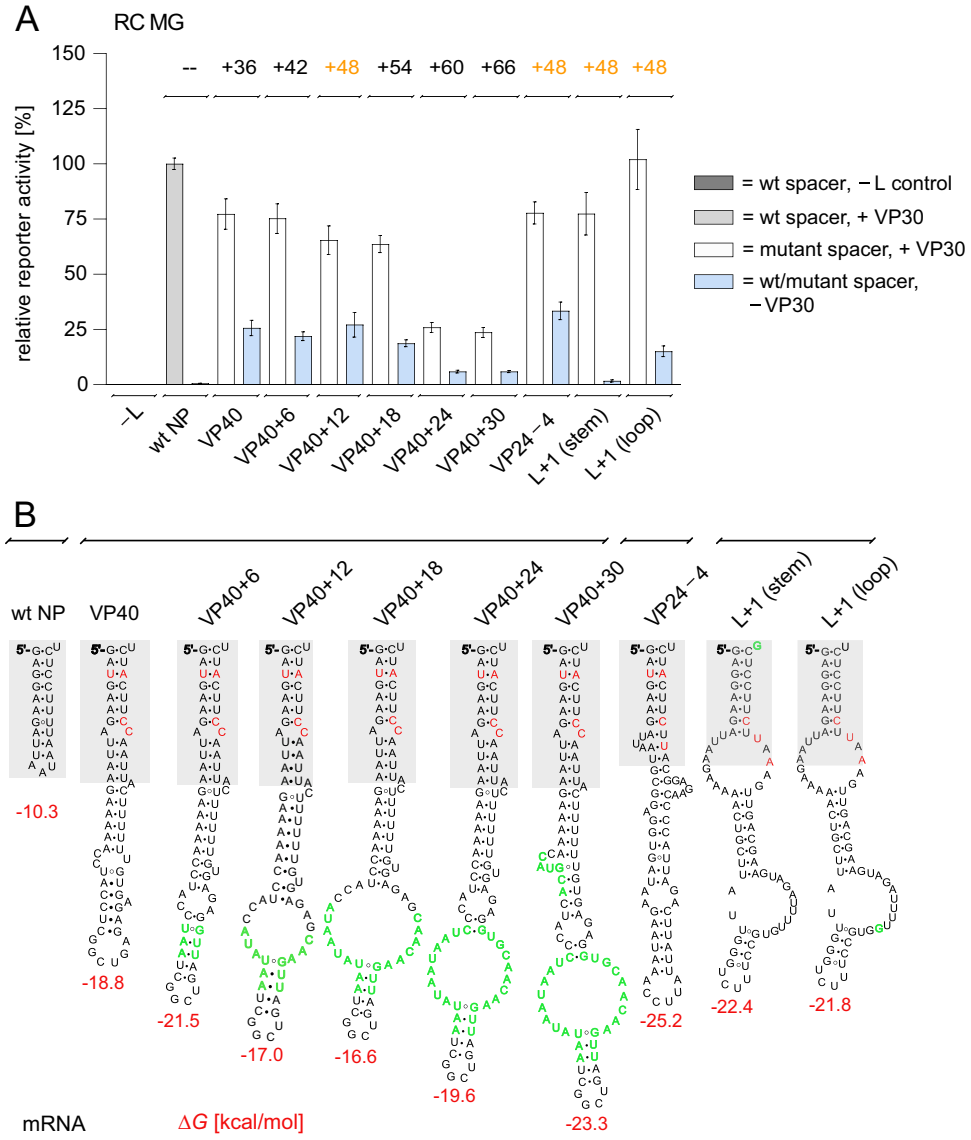

FIG 7 Influence of hairpin/spacer length on VP30-independent transcription. (A) Luciferase reporter gene assays of monocistronic RC MGs comprising the VP40 HP and mutant variants thereof. The VP40 hairpin was elongated in steps of 6 nt. The MG variants VP24−4, L+1 (stem), and L+1 (loop) were included as well to represent different sequence contexts. Numbers above the columns indicate the numbers of nucleotides that were inserted into the spacer relative to the wt NP MG. Numbers are shown in orange for variants with a different sequence context but the same spacer expansion of 48 nt. (B) Hairpin structures predicted to form at the mRNA 5′ ends of the MGs analyzed in panel A. ΔG values are those of the MFE structure predicted by RNAfold using the default parameters (for more details, see the legend to Fig. 1A). Nucleotides inserted into the EBOV-specific hairpin sequences are in green. Nucleotide positions in the lower hairpin stem regions (gray boxes) that deviate from the wt NP stem sequence are in red.

(loop) (Fig. 2A)] or the 1-nt insertion in the L+1 (stem) that moves the base of the genomic hairpin stem 1 nt away from PE2 is responsible for the difference.

DISCUSSION

At the onset of this study, our state of knowledge was entirely based on the phenotype of the NheI HP mutant (15). The key conclusion of that study was that destabilization of the NP HP structure particularly at the positive-sense RNA level makes mRNA synthesis VP30 independent, while transcription in the presence of the native NP HP is strictly VP30 dependent. This led the authors to suggest that a stably forming hairpin

structure at the TSS defines the VP30 dependency of transcription (15). Using an enlarged series of mutant MGs and not only reporter assays but also qRT-PCR for sensitive quantifications of viral RNA species, we were able to differentiate, refine, and contextualize this initial model.

Our study has revealed that the phenotype of the NheI NP mutant is less distinct and unequivocal than previously assumed. This mutant relaxes the VP30 dependency of transcription only partially (Fig. 5D; ~4-fold increased relative to the wt NP MG), but even the wt NP MG gives rise to residual VP30-independent transcription above background (Fig. 5D), which has remained unrecognized so far. Also, in our setup, mRNA levels in the presence of VP30 were somewhat reduced for the NheI NP mutant compared with the wt NP construct (Fig. 5D), while the previous Northern blot analysis instead suggested increased levels (15). These discrepancies may be related to different sensitivities of the methods used but may also suggest increased fluctuation of viral mRNA levels in cells transfected with the NheI NP MG.

Most deviations from the NP HP structure, provided that they did not further stabilize the stem structure, relaxed the VP30 control of transcription partially and to different extents, but none made this process entirely VP30 independent. Even the Δ5′ spacer mutant, lacking any potential to form secondary structures at the TSS on the genomic or antigenomic level, remained largely VP30 dependent (Fig. 3). One possibility is that VP30 supports one or a few conformational steps in the viral polymerase complex that help the enzyme to establish and/or maintain its transcription mode. With some variants of the PE1-PE2 spacer regions, such as construct VP35+1 (loop) v2, a larger fraction of polymerases may be able to traverse this switch without VP30, but the conformational equilibrium cannot be entirely driven to the transcription-competent state without VP30. VP30 was shown *in vitro* to bind RNA quite promiscuously (13), which is consistent with our finding that VP30 was able to act on a variety of spacer variants that differed in sequence, structure, and length. However, it should be considered that potential differences in VP30 affinity for the various 3′-leader RNAs may have been masked by saturating VP30 expression levels in the MG system. As a result, the tolerance to RNA changes in the spacer region of the 3′-leader promoter may be more restricted in infections by full-length virus.

Stabilization of RNA secondary structure at the TSS (variants NP G_{-72}, $VP40_6$, and $VP40_5$), as low as a few kilocalories per mole in the case of mutant NP G_{-72}, tightened the VP30 dependency but simultaneously reduced mRNA and cRNA synthesis and attenuated the increase of cRNA synthesis upon omission of VP30 (Fig. 4C and D). A straightforward explanation is that fewer polymerases were able to productively bind the genomic promoter, possibly because VP35 had difficulties in resolving such stabilized duplex regions via its recently described RNA helicase activity (18). Second, the attenuated switch to replication in the absence of VP30 may suggest that structural stabilizations at the TSS prevent the polymerase complex from redirecting itself to the genome 3′ end for initiation of cRNA synthesis. Altogether, it has become evident from our findings that the NP hairpin structure at the TSS, which is slightly less stable than our NP G_{-72} mutant, is optimized for viral RNA synthesis in terms of balancing transcription efficiency and tightness of VP30 dependency, as well as supporting the polymerase's capacity to increase cRNA synthesis when VP30 is absent.

Making the UN_5 hexamer phasing continuous between PE1 and PE2 (variants NP U_{-75} and NP U_{-75}/G_{-72}), which concomitantly weakened the HP structure relative to the wt NP and NP G_{-72} constructs (Fig. 5A), boosted transcription activity (Fig. 5B to D, +VP30 and −VP30). Furthermore, cRNA synthesis was increased in the presence of VP30, but the switch from transcription to replication in the absence of VP30 was dysregulated (Fig. 5E). On the one hand, this phenotype emphasizes the important function of UN_5 hexamer phasing in supporting RdRp activity at the 3′-leader promoter, which is likely intertwined with NP-RNA binding (17). On the other hand, this unleashed RdRp transcription activity is associated with a loss of regulation of viral RNA synthesis. The high similarity of the phenotypes of mutants NP U_{-75} and NP U_{-75}/

G_{-72} is also surprising, considering that the additional G_{-72} mutation largely compensated for the loss of structure caused by the U_{-75} mutation *per se* (Fig. 5A). Finally, the base of the stem is predicted to be extended by two A·U bp in the NP U_{-75} and NP U_{-75}/G_{-72} mutants (Fig. 5A), thus potentially including nucleotides of PE1 and PE2 in stem formation on the genomic RNA level. At present, we cannot exclude the possibility that this feature may have contributed to the phenotype of the two mutants. The positioning of the predicted stem base with respect to PE1 and PE2 is something that needs to be explored in more detail, as illustrated by the distinct VP30 dependency of the L+1 (stem) versus L+1 (loop) variants (Fig. 3A and C).

UN_5 hexamer phasing is also continuous in variants VP35+1 (stem) and Δ5′ spacer (Fig. 2), but their transcription activity in the absence of VP30 (Fig. 3C) was lower than for the NP U_{-75}, and U_{-75}/G_{-72} mutants (Fig. 5D). Thus, other features seem to limit VP30-independent transcription of the two latter variants. This may be the 12-nt deletion between PE1 and PE2 in the Δ5′ spacer mutant and the single-nucleotide insertion between the HP stem and PE2 in variant VP35+1 (stem). In comparison, variant VP35+1 (loop) v2, sharing the same spacer length and a very similar HP structure with variant VP35+1 (stem) (Fig. 2), has one interruption of UN_5 hexamer phasing between PE1 and PE2 (as the wt NP HP) but showed the highest levels of VP30-independent transcription (45% [Fig. 3C]) of all tested MG constructs. Evidently, further investigations are required to understand the UN_5 hexamer code, its sequence constraints, its intertwining with RNA structure at the TSS, and the molecular functions it encodes.

Low residual mRNA, cRNA, and vRNA synthesis can occur in the case of MG constructs disrupting hexamer periodicity [variants VP35 and NP-1 (stem)]. The extent depends on the sequence/structure context, and low-efficiency mRNA synthesis is stimulated by VP30 (Fig. 6B). It is unclear why the VP35 construct was more efficient than the NP-1 (stem) construct. One possibility is that the 1-nt deletion in the latter construct changes HP stem distance to PE2, as discussed above. Other mutants, such as NP mutants with the 1-nt deletion in the loop, could be analyzed to test this possibility. Another testable possibility is that the third base pair of the genomic HP stem, which is C·G in the NP and A·U in the VP35 HP (Fig. 6A), plays a key role in this context.

Two recent structural and mutational studies characterized the interaction between the C-terminal domain of VP30 (amino acids [aa] ~140 to 280) and a stretch of residues in the C-terminal portion of NP (aa 600 to 614) (21, 22). In one of the studies (22), this interaction, depending on the key residue W230 of VP30, was found to be crucial for viral RNA synthesis in the presence of the native NP hairpin at the TSS but not for transcription initiation in the presence of the NheI mutant HP. The authors concluded from their results that there are components of EBOV RNA synthesis that depend on this VP30-NP interaction, while others do not (22). This suggests that VP30 has multiple functions in the RdRp complex, likely defined by the protein's multiple interfaces with the RNA, VP35 (via RNA bridging [12]), NP, and possibly L itself (23). These various VP30 interactions may help orchestrate the conformational steps that are carried out during viral RNA synthesis, resulting in highly efficient transcription initiation and stabilization of elongating transcription complexes. This view is consistent with our observations that a low level of VP30-independent transcription even takes place with MGs carrying the native 3′-leader, but none of our mutant constructs gave rise to equal transcription efficiency in the absence versus presence of VP30.

The study by Kirchdoerfer et al. (21) analyzed the consequences of affinity-up and affinity-down mutations at the NP binding interface of VP30. For example, the VP30 P206R mutation enhancing affinity for NP decreased viral polymerase activity in an MG assay, while the D202R mutation, which moderately decreased this affinity, boosted activity to levels markedly above that obtained with wt VP30. More severe affinity loss mutations again decreased RNA synthesis activity to (almost) background levels (21). The authors proposed that high-affinity VP30-NP interactions may support the recruitment of VP30 to cellular NP inclusions but may rigidify the nucleocapsid and thereby restrict access of the viral polymerase to the viral genome. VP30 mutations that

modestly reduce affinity to NP may facilitate access of the polymerase to the viral genome, without critically compromising other aspects of VP30 function. Severe reductions in VP30-NP affinity may disable the incorporation of VP30 into RNA synthesis complexes.

Conclusions. Our study demonstrates that any changes in the PE1-PE2 spacer of the EBOV 3′-leader promoter in terms of RNA sequence, hexamer phasing, structure formation potential, and length alter the tightness of VP30 control of transcription and/or overall efficiency of transcription (and replication) and/or dampen the induction of replication in the absence of VP30. Thus, the native EBOV spacer region is evolutionarily optimized for balanced and efficient viral transcription and replication under tight regulation by VP30. The comprehensive set of spacer variants analyzed here has identified key mutants and has opened up perspectives for additional strategic spacer mutants to eventually be tested in recombinant full-length EBOV, aiming at dissecting the molecular basis of regulation of EBOV transcription and replication. Our findings support the notion that the molecular basis, still far from being understood, is an intricate interplay of RNA sequence and structure, spacer length, and UN_5 hexamer periodicity in the EBOV 3′-leader promoter, which impacts the orchestration of multiple RNA-protein and possibly also protein-protein interactions.

MATERIALS AND METHODS

Cell culture. HEK293 cells (DSMZ ACC 305) were cultivated at 37°C and 5% CO_2 in a humidified atmosphere in Dulbecco's modified Eagle medium (DMEM) containing 10% fetal calf serum (FCS), 50 U/ml penicillin, 50 μg/ml streptomycin, and 2 mM L-glutamine (Thermo Fisher Scientific [TFS]). Propagation of plasmid DNA was performed using the *Escherichia coli* DH5α strain and applying standard microbiological procedures.

Plasmids. Minigenomes (MGs) with mutations in the 3′-leader promoter were constructed as described previously (17). Plasmids encoding the MG variants as well as pCAGGS-derived plasmids coding for the Zaire EBOV nucleocapsid proteins (VP30, NP, VP35, and L) and the T7 RNA polymerase (17, 24, 25) were cotransfected into HEK293 cells (see below), together with plasmid pGL4.13 encoding firefly luciferase (Promega), which was used as a transfection control.

Transfection of the EBOV-specific minigenome system. HEK293 cells, 8×10^5 per well, were seeded into 6-well plates (Greiner) 18 to 24 h before transfection and were cultivated at 37°C and 5% CO_2 in the DMEM specified above (3 ml/well). Transfection of MG assay plasmids was performed as described previously (17). Briefly, plasmids encoding the EBOV nucleocapsid proteins NP (125 ng), VP35 (125 ng), VP30 (100 ng), and L (1,000 ng), a T7 promoter-driven EBOV-specific MG variant encoding *Renilla* luciferase (250 ng), a plasmid encoding T7 RNA polymerase (250 ng), and pGL4.13 (Promega), encoding firefly luciferase, were cotransfected into HEK293 cells using the TransIT-LT1 transfection reagent (Mirus) according to the manufacturer's instructions. Cells were harvested 48 h posttransfection, and lysates were used for either luciferase reporter gene activity measurements or total RNA extraction followed by qRT-PCR.

Luciferase assay. Reporter gene activities were measured in separate *Renilla* and firefly luciferase assays (PJK Biotech) as described earlier (17) using a Centro LB 960 luminometer (Berthold Technologies). *Renilla* luciferase activity values were normalized to those for firefly luciferase (FF) values to account for potential differences in transfection efficiency. Normalized activity values obtained for RC or RD MGs carrying the native 3′-leader were set to 100%.

Quantitative and strand-specific real-time PCR. (i) RNA extraction and purification. Total RNA was isolated from cells transfected with EBOV-specific MGs using the RNeasy minikit (Qiagen) according to the manufacturer's instructions. An on-column digestion using an RNase-free DNase set (Qiagen) was included. A second DNase treatment in solution was performed using Ambion DNase I in the presence of the RiboLock RNase inhibitor (both from TFS), as detailed in reference 17.

(ii) Reverse transcription. Reverse transcription was conducted as described previously (17). Briefly, 500 ng RNA was used for reverse transcription (RT) (Fig. 1) of either vRNA [primer luc(+), 5′-GGC CTC TTC TTA TTT ATG GCG A-3′], cRNA (primer RT_cRNA, 5′-CAG TCC TGC CTT TTC TTT TAA TTT TAT C-3′), positive-strand RNAs [cRNA/mRNA; primer luc(−), 5′-AGA ACC ATT ACC AGA TTT GCC TGA-3′] (illustrated in Fig. 8; RT primers in red) or firefly luciferase mRNA (internal control; using the Random Hexamer Primer mixture [TFS]). Reactions were performed with the RevertAid H Minus reverse transcriptase (TFS) according to the manufacturer's protocol in a total reaction volume of 20 μl.

(iii) Quantitative real-time PCR. Quantitative real-time PCR was performed as described previously (17). Briefly, ~5 ng cDNA was amplified in a total volume of 10 μl on a QuantStudio3 real-time PCR system (TFS) using the PowerUp SYBR green master mix (TFS) following the manufacturer's fast-cycling-mode protocol. vRNA and positive-sense RNA (cRNA and mRNA) were amplified by a combination of the RT primers luc(+) and luc(−); specific amplification of cRNA was performed using primers RT_cRNA (see above) and cRNA_fwd (5′- CGG TGA TAG CCT TAA TCT TTG TG-3′) (Fig. 8). For amplification of firefly luciferase mRNA, primers qPCR_FF_fwd (5′-CGT GCA AAA GAA GCT ACC G-3′) and qPCR_FF_rev (5′-GGT GGC AAA TGG GAA GTC AC-3′) were used. RNA levels were quantified by the $2^{-\Delta\Delta C_T}$ method (see below).

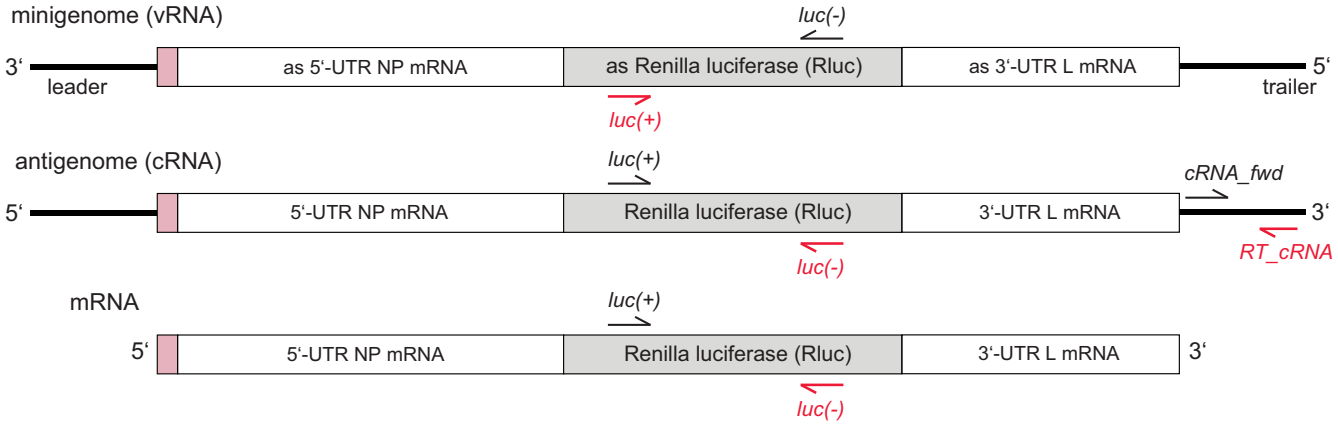

FIG 8 Schematic representation of primers used for qRT-PCR of viral RNA species. RT primers are in red. as, antisense. The box representing the first NP hairpin structure is pink (see also Fig. 1).

(iv) Quantification and statistical analysis. For one biological replicate, three wells of a 6-well plate (Greiner) were seeded in parallel with 8×10^5 HEK293 cells each and transfected with the specific MG plasmid and pCAGGS-derived support plasmids (with and without the VP30 plasmid) described above. From these three technical replicates each, two identical cDNA samples (after reverse transcription) were analyzed by qPCR, resulting in a total of six cycle threshold (C_T) values obtained per biological replicate and MG variant (with and without VP30). For subsequent calculations, the mean C_T value of the two qPCR replicates was used. For each technical replicate individually, we calculated the ΔC_T value by subtracting the C_T value for firefly luciferase mRNA from that of the specific viral RNA species. For determination of mRNA levels, $2^{-\Delta C_T}$ values for cRNA were subtracted from those for cRNA+mRNA (RT-PCR efficiencies were determined as 1.98 for cRNA and 2.00 for cRNA+mRNA [17]). $\Delta\Delta C_T$ values were calculated by subtracting the mean ΔC_T value of the three technical replicates for the wt NP construct from the ΔC_T value of the individual technical replicate of the mutant MG, the −L, control or the wt NP MG itself. From the resulting $2^{-\Delta\Delta C_T}$ values (3 for each biological replicate), the mean $2^{-\Delta\Delta C_T}$ value and the standard error of the mean (SEM) were derived. GraphPad Prism version 8.1.1 for Windows was used for further data processing. *P* values are defined in the figure legends; the unpaired *t* test with Welch's correction was applied.

SUPPLEMENTAL MATERIAL

Supplemental material is available online only.

SUPPLEMENTAL FILE 1, PDF file, 0.3 MB.

ACKNOWLEDGMENTS

We acknowledge experimental and technical support by Astrid Herwig (cell culture) and Jana Schneider (minigenome assays).

This work was funded by Deutsche Forschungsgemeinschaft (DFG) (CRC 1021, project A02).

REFERENCES

1. Rougeron V, Feldmann H, Grard G, Becker S, Leroy EM. 2015. Ebola and Marburg haemorrhagic fever. J Clin Virol 64:111–119. https://doi.org/10.1016/j.jcv.2015.01.014.
2. Burk R, Bollinger L, Johnson JC, Wada J, Radoshitzky SR, Palacios G, Bavari S, Jahrling PB, Kuhn JH. 2016. Neglected filoviruses. FEMS Microbiol Rev 40:494–519. https://doi.org/10.1093/femsre/fuw010.
3. Mehedi M, Falzarano D, Seebach J, Hu X, Carpenter MS, Schnittler H-J, Feldmann H. 2011. A new Ebola virus nonstructural glycoprotein expressed through RNA editing. J Virol 85:5406–5414. https://doi.org/10.1128/JVI.02190-10.
4. Mühlberger E. 2007. Filovirus replication and transcription. Future Virol 2:205–215. https://doi.org/10.2217/17460794.2.2.205.
5. Deflubé LR, Cressey TN, Hume AJ, Olejnik J, Haddock E, Feldmann F, Ebihara H, Fearns R, Mühlberger E. 2019. Ebolavirus polymerase uses an unconventional genome replication mechanism. Proc Natl Acad Sci U S A 116:8535–8543. https://doi.org/10.1073/pnas.1815745116.
6. Albariño CG, Guerrero LW, Chakrabarti AK, Nichol ST. 2018. Transcriptional analysis of viral mRNAs reveals common transcription patterns in cells infected by five different filoviruses. PLoS One 13:e0201827-13. https://doi.org/10.1371/journal.pone.0201827.
7. Shabman RS, Jabado OJ, Mire CE, Stockwell TB, Edwards M, Mahajan M, Geisbert TW, Basler C. 2014. Deep sequencing identifies noncanonical editing of Ebola and Marburg virus RNAs in infected cells. mBio 5:e02011-14. https://doi.org/10.1128/mBio.02011-14.
8. Feldmann H, Mühlberger E, Randolf A, Will C, Kiley MP, Sanchez A, Klenk HD. 1992. Marburg virus, a filovirus: méssenger RNAs, gene order, and regulatory elements of the replication cycle. Virus Res 24:1–19. https://doi.org/10.1016/0168-1702(92)90027-7.
9. Mühlberger E, Weik M, Volchkov VE, Klenk HD, Becker S. 1999. Comparison of the transcription and replication strategies of Marburg virus and Ebola virus by using artificial replication systems. J Virol 73:2333–2342. https://doi.org/10.1128/JVI.73.3.2333-2342.1999.
10. Sanchez A, Kiley MP. 1987. Identification and analysis of ebola virus messenger RNA. Virology 157:414–420. https://doi.org/10.1016/0042-6822(87)90283-2.

11. Biedenkopf N, Lier C, Becker S. 2016. Dynamic phosphorylation of VP30 is essential for Ebola virus life cycle. J Virol 90:4914–4925. https://doi.org/10.1128/JVI.03257-15.
12. Biedenkopf N, Schlereth J, Grünweller A, Becker S, Hartmann RK. 2016. RNA binding of Ebola virus VP30 is essential for activating viral transcription. J Virol 90:7481–7496. https://doi.org/10.1128/JVI.00271-16.
13. Schlereth J, Grünweller A, Biedenkopf N, Becker S, Hartmann RK. 2016. RNA binding specificity of Ebola virus transcription factor VP30. RNA Biol 13:783–798. https://doi.org/10.1080/15476286.2016.1194160.
14. Biedenkopf N, Hartlieb B, Hoenen T, Becker S. 2013. Phosphorylation of Ebola virus VP30 influences the composition of the viral nucleocapsid complex. J Biol Chem 288:11165–11174. https://doi.org/10.1074/jbc.M113.461285.
15. Weik M, Modrof J, Klenk HD, Becker S, Mühlberger E. 2002. Ebola virus VP30-mediated transcription is regulated by RNA secondary structure formation. J Virol 76:8532–8539. https://doi.org/10.1128/jvi.76.17.8532-8539.2002.
16. Weik M, Enterlein S, Schlenz K, Muhlberger E. 2005. The Ebola virus genomic replication promoter is bipartite and follows the rule of six. J Virol 79:10660–10671. https://doi.org/10.1128/JVI.79.16.10660-10671.2005.
17. Bach S, Biedenkopf N, Grünweller A, Becker S, Hartmann RK. 2020. Hexamer phasing governs transcription initiation in the 3'-leader of Ebola virus. RNA 26:439–453. https://doi.org/10.1261/rna.073718.119.
18. Shu T, Gan T, Bai P, Wang X, Qian Q, Zhou H, Cheng Q, Qiu Y, Yin L, Zhong J, Zhou X. 2019. Ebola virus VP35 has novel NTPase and helicase-like activities. Nucleic Acids Res 47:5837–5851. https://doi.org/10.1093/nar/gkz340.
19. Bach S, Demper JC, Biedenkopf N, Becker S, Hartmann RK. 2020. RNA secondary structure at the transcription start site influences EBOV transcription initiation and replication in a length- and stability-dependent manner. RNA Biol 22:1–14. https://doi.org/10.1080/15476286.2020.1818459.
20. Cordey S, Roux L. 2007. Further characterization of a paramyxovirus transcription initiation signal: search for required nucleotides upstream and importance of the N phase context. J Gen Virol 88:1555–1564. https://doi.org/10.1099/vir.0.82701-0.
21. Kirchdoerfer RN, Moyer CL, Abelson DM, Saphire EO. 2016. The Ebola virus VP30-NP interaction is a regulator of viral RNA synthesis. PLoS Pathog 12:e1005937. https://doi.org/10.1371/journal.ppat.1005937.
22. Xu W, Luthra P, Wu C, Batra J, Leung DW, Basler CF, Amarasinghe GK. 2017. Ebola virus VP30 and nucleoprotein interactions modulate viral RNA synthesis. Nat Commun 8:15576. https://doi.org/10.1038/ncomms15576.
23. Groseth A, Charton JE, Sauerborn M, Feldmann F, Jones SM, Hoenen T, Feldmann H. 2009. The Ebola virus ribonucleoprotein complex: a novel VP30-L interaction identified. Virus Res 140:8–14. https://doi.org/10.1016/j.virusres.2008.10.017.
24. Hoenen T, Groseth A, Kolesnikova L, Theriault S, Ebihara H, Hartlieb B, Bamberg S, Feldmann H, Ströher U, Becker S. 2006. Infection of naïve target cells with virus-like particles: implications for the function of Ebola virus VP24. J Virol 80:7260–7264. https://doi.org/10.1128/JVI.00051-06.
25. Hoenen T, Jung S, Herwig A, Groseth A, Becker S. 2010. Both matrix proteins of Ebola virus contribute to the regulation of viral genome replication and transcription. Virology 403:56–66. https://doi.org/10.1016/j.virol.2010.04.002.
26. Calain P, Monroe MC, Nichol ST. 1999. Ebola virus defective interfering particles and persistent infection. Virology 262:114–128. https://doi.org/10.1006/viro.1999.9915.
27. Lorenz R, Bernhart SH, Höner zu Siederdissen C, Tafer H, Flamm C, Stadler PF, Hofacker IL. 2011. ViennaRNA package 2.0. Algorithms Mol Biol 6:26. https://doi.org/10.1186/1748-7188-6-26.